Topology optimization for fluid flows using the MPS method incorporating the level set method

Y. Sasaki[a], Y. Sato[a], T. Yamada[a,*], K. Izui[a], S. Nishiwaki[a]

[a] *Department of Mechanical Engineering and Science, Kyoto University, Kyoto 615-8540, Japan.*

Abstract

Topology optimization for fluid field problems has been studied for many years, but most of them use the Eulerian coordinate system in the numerical analysis methods such as the finite element method and the finite volume method. The moving particle semi-implicit (MPS) method is one of the particle methods, which can be used to analyze incompressible free surface fluid flows. The MPS method is a meshless method based on the Lagrangian coordinate system without surface tracking by a mesh or a scalar quantity. It has attracted attention in recent years since this has several advantages such as the easy expression of the free boundaries. This paper presents a new topology optimization method for fluid dynamics problems using the MPS method. First, the optimization problems are formulated based on the level set method and the MPS method. Next, the design sensitivities are derived using the Lagrange multiplier method and adjoint variable method. The optimization algorithm is constructed based on those formulations, and the validity and the availability of the proposed method are confirmed through several numerical examples.

Keywords: Topology Optimization, MPS method, Level set method, Sensitivity Analysis

*Corresponding author
Email address: takayuki@me.kyoto-u.ac.jp (T. Yamada)

1. Introduction

Topology optimization[1, 2, 3] is the most flexible structural optimization method that allows the topological changes such as introduction of the holes as well as the shape changes, and has a potential to explore the high performance structures. The basic idea of topology optimization is the introduction of a fixed design domain that is composed of the original design domain consisting of material, and void domains [1]. Using the characteristic function originally presented in the papers of Murat and Tartar [4], the optimization problem is replaced with a material distribution problem. Topology optimization was originally proposed as the so-called homogenization design method [1] where the homogenization method is used for the relaxation of the design domain. The density approach [5], also called the solid isotropic material with penalization (SIMP) method, is currently the most popular topology optimization approach. The idea of the density approach is the use of a fictitious isotropic material whose elasticity tensor is supposed to be a function of penalized material density, expressed as an exponent parameter. Using the density of continuously changing material as design variables, the optimal density distribution in the design domain is determined by minimizing the objective function. In addition, the level set-based approach [6, 7, 8] where the boundaries of the target domain are moved according to the shape sensitivities on the boundaries for each optimization iteration, and evolutionary [9] approaches have been proposed.

Based on the density approach, topology optimization of fluid dynamics problems was pioneered by Borrvall and Petersson [10] for minimization of viscous dissipation in a Stokes flow problem, where the material distribution in the fixed design domain is expressed as either the presence of fluid or an impermeable solid domain. In research based on this methodology, a topology optimization method for large-scale Stokes flow problems was proposed by Aage et al. [11]. Olesen et al.[12] proposed a topology optimization method using the steady-state Navier-Stokes equations for incompressible fluids, and introduced a numerical implementation scheme using commercial software. Deng et al.[13],

and Kreissl and Maute [14], proposed a topology optimization method using the unsteady Navier-Stokes equations for incompressible fluids. A topology optimization of turbulent flows was proposed by Dilgen et al. [15, 16]. Yaji et al. [17] , Dugas et al. [18] and Norgaard et al. [19] proposed a topology optimization method for fluid flow problems using the lattice Boltzmann method. Although there are a lot of papers on topology optimization for fluid problems as described above, they are not on topology optimization for free surface flows

As a different type of structural optimization method, structural optimization methods [20, 21, 22, 23] using a level set method have been proposed. In such methods, structural configurations are implicitly represented using the isosurface of the level set function[24], which is a scalar function. A level set-based structural optimization method for minimum power dissipation problems under Stokes flow was proposed by Challis and Guest [25]. Duan et al. [26], Zhou et al. [27], and Duan et al. [28] proposed a level set-based structural optimization method for steady-state Navier-Stokes flow problems, and Deng et al.[29] extended it to unsteady Navier-Stokes flow optimization problems. However, since these level set-based structural optimization methods are essentially constructed based on the concept of shape optimization methods that obtain optimal configurations by moving structural boundaries, they do not allow topological changes such as the creation of new boundaries during the optimization procedure. On the other hand, a level set-based approach proposed by Yamada et al. [30] is constructed based on the concept of the topology optimization described above, and allows the topological changes during the optimization procedure and overcomes the above problems. This uses topological derivatives and a reaction-diffusion equation for updating the level set function. This method was applied to topology optimization of fluid dynamics problems [31, 32].

The most common topology optimization for fluid dynamics problems introduces the Eulerian coordinate systems in the numerical analysis methods such as the finite element method (FEM) [10] , and the finite volume method (FVM) [33] where they are well known common analysis techniques developed in the fluid mechanics field. However, due to characteristics of these numerical meth-

ods, when dealing with fluid dynamics problems with free surface flows, specific techniques for representing their boundaries such as the level set method must be introduced, and the calculation cost may be enormous.

The Moving particle semi-implicit (MPS) method [34] is one of the particle methods widely studied, because it does not need explicit surface tracking by a mesh or a scalar quantity and it is suitable for analysis of fluid fields with the movements of free boundaries. In the FEM [35, 36] and Lattice Boltzmann method [37], when analyzing free surface flows, advanced techniques and ideas are necessary, and numerical oscillation may occur when calculating the convection term in the Navier-Stokes equation. However, in the MPS method, it is easier to express free surface boundary and there is no particular problem in calculating free surface flows.

The MPS method is a macroscopic deterministic Lagrangian meshless method originally proposed for the analysis of incompressible free surface flows. There are other particle methods like the smooth particle hydrodynamics (SPH) method [38, 39]. Both the MPS method and SPH method provide approximations to the strong form of the partial differential equations (PDEs) on the basis of integral interpolants. The MPS method applies simplified differential operator models based on local weighted averaging processes, while in the SPH method, the PDEs are calculated based on the gradient of a kernel function. During the past years, the MPS method has been proven to be useful in a wide range of engineering fields, such as nuclear engineering [40, 41, 42, 43], coastal engineering [44, 45, 46], ocean engineering [47, 48, 49], hydraulic engineering [50, 51], structural engineering [52], mechanical engineering [53, 54], bioengineering [55, 56] and chemical engineering [57].

In this paper, we propose a topology optimization method using the level set method and the MPS method for fluid dynamics problems that has a potential to deal with the free boundaries without surface tracking methods. In the following sections, we briefly explain formulations and implementation techniques of the MPS method and topology optimization at first. Next, optimization problems are formulated based on the level set-based topology optimization method

and the MPS method. Then, the design sensitivity analysis, performed using the adjoint variable method, is explained, and we describe the numerical implementation. Finally, numerical examples are provided to confirm the validity and utility of the proposed method.

2. MPS method

The MPS method is one of the particle methods, which can be used to analyze incompressible free surface flows without surface tracking. In the MPS method, the motion of the continuum is described as the motion of a finite number of particles. Each particle is calculated through interactions with neighboring particles covered with the weight function. The MPS method is the Lagrangian method and does not require meshes unlike Eulerian methods such as the finite element method or the finite volume method. Thus, we can avoid calculating the convection term in Navier-Stokes equation, which causes numerical diffusion and oscillation. This mesh-less numerical approach, proposed by Koshizuka, et al [34] has been proven to be useful in a wide range of engineering applications, such as numerical analysis of turbines and mixers.

In this section, we discuss the concept of the MPS method, which is applied to incompressible flows.

2.1. Governing equations

The governing equations of the MPS method are the continuity and the Navier-Stokes equations as follows:

$$\frac{1}{\rho}\frac{D\rho}{Dt} = -\nabla \cdot \boldsymbol{u}, \tag{1}$$

$$\frac{D\boldsymbol{u}}{Dt} = -\frac{1}{\rho}\nabla p + \nu\nabla^2\boldsymbol{u} + \boldsymbol{f}, \tag{2}$$

where $\boldsymbol{u}$ is the fluid velocity; p is the pressure; ρ is the fluid density; ν is the fluid kinematic viscosity; and $\boldsymbol{f}$ is the body force loaded on the flow. In the MPS method, the left side of the continuity and the Navier-Stokes equations denote the Lagrangian differentiation. Therefore, it is not necessary to calculate the

convection term in the Navier-Stokes equation, and in the continuity equation, we use the constant density condition of the fluid.

2.2. Modeling of gradient and Laplacian

In the MPS method, we represent differential operators such as the gradient and Laplacian with the particle interaction model (Fig.1), and discretize the differential equations using this model. In this model, each particle interacts with other particles with weight function $w(r)$, where r is the distance between two particles and r_e is the effective radius. We use the following function as the weight function in Eq.(3) (Fig.2):

$$w(r) = \begin{cases} 1 - 6\left(\frac{r}{r_e}\right)^2 + 8\left(\frac{r}{r_e}\right)^3 - 3\left(\frac{r}{r_e}\right)^4 & (0 \leq r < r_e) \\ 0 & (r_e \leq r) \end{cases}. \tag{3}$$

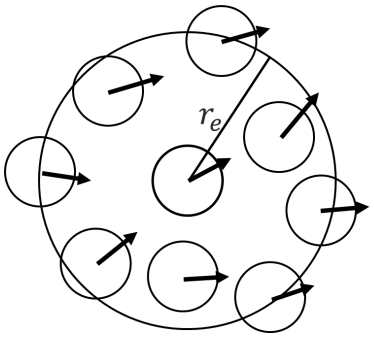

Figure 1: Particle interaction

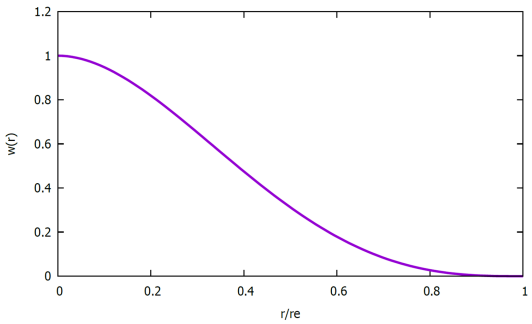

Figure 2: Weight function

We define particle number density as follows:

$$n_i = \sum_{j \neq i} w(|\boldsymbol{r}_j - \boldsymbol{r}_i|). \tag{4}$$

The particle number density of the internal fluid region should be constant to satisfy the continuity equation, Eq.(1). The parameter n_0 denotes the constant particle number density of internal particles in the initial condition.

The gradient and Laplacian models are represented using particle number density as follows:

$$\langle \nabla \phi \rangle_i = \frac{d}{n^0} \sum_{j \neq i} \left[\frac{\phi_j - \phi_i}{|\boldsymbol{r}_j - \boldsymbol{r}_i|^2} (\boldsymbol{r}_j - \boldsymbol{r}_i) w(|\boldsymbol{r}_j - \boldsymbol{r}_i|) \right], \tag{5}$$

$$\langle \nabla^2 \phi \rangle_i = \frac{2d}{\lambda^0 n^0} \sum_{j \neq i} (\phi_j - \phi_i) w(|\boldsymbol{r}_j - \boldsymbol{r}_i|). \tag{6}$$

where d is the number of space dimensions. The constant parameter λ^0 is given as follows:

$$\lambda^0 = \frac{\sum_{j \neq i} |\boldsymbol{r}_j^0 - \boldsymbol{r}_i^0|^2 w(|\boldsymbol{r}_j^0 - \boldsymbol{r}_i^0|)}{\sum_{j \neq i} w(|\boldsymbol{r}_j^0 - \boldsymbol{r}_i^0|)}. \tag{7}$$

This parameter corrects the variance increase of the Laplacian model so that the variance agrees with that of the analytical solution.

2.3. Semi-implicit algorithm of MPS method

The MPS method employs the fractional step algorithm where a one-time step is divided into two processes. We divide the Navier-Stokes equation into two parts as follows:

$$\frac{\boldsymbol{u}_i^* - \boldsymbol{u}_i^k}{\Delta t} = \nu \langle \nabla^2 \boldsymbol{u} \rangle_i^k + \boldsymbol{f}, \tag{8}$$

$$\frac{\boldsymbol{u}_i^{k+1} - \boldsymbol{u}_i^*}{\Delta t} = -\frac{1}{\rho^0} \langle \nabla p \rangle_i^{k+1}, \tag{9}$$

where ρ^0 is the fluid density of the initial condition and we differentiate ρ^0 from ρ^* which is the fluid temporal density of the state where the incompressibility is not satisfied, and $\boldsymbol{u}^*$ is the temporal velocity. In the first process, from Eq.(8), the temporal velocities and positions are obtained explicitly (at time step k) as follows:

$$\boldsymbol{u}_i^* = \boldsymbol{u}_i^k + [\nu \langle \nabla^2 \boldsymbol{u} \rangle_i^k + \boldsymbol{f}] \Delta t, \tag{10}$$

$$\boldsymbol{r}_i^* = \boldsymbol{r}_i^k + \boldsymbol{u}_i^* \Delta t. \tag{11}$$

In the second process, the following Poisson equation of pressure derived from Eq.(1) and Eq.(9) is solved implicitly:

$$\langle \nabla^2 p \rangle_i^{k+1} = -\rho^0 \frac{1}{(\Delta t)^2} \frac{n_i^* - n^0}{n^0}, \tag{12}$$

where n^* is the temporal particle number density after the first process. The source term represents the deviation of the temporary particle number density from the constant particle number density. Then, velocity correction from the pressure term is calculated and the new-time velocity and position are modified as follows:

$$\boldsymbol{u}_i' = -\frac{\Delta t}{\rho^0} \langle \nabla p \rangle_i^{k+1}, \tag{13}$$

$$\boldsymbol{u}_i^{k+1} = \boldsymbol{u}_i^* + \boldsymbol{u}_i', \tag{14}$$

$$\boldsymbol{r}_i^{k+1} = \boldsymbol{r}_i^k + \boldsymbol{u}_i^{k+1} \Delta t. \tag{15}$$

2.4. Boundary conditions using MPS method

In order to calculate the governing equations and the adjoint equations in optimization problems, we have to set boundary conditions. However, because the MPS method is the Lagrangian method, it is more difficult to set boundary conditions using the MPS method than using Eulerian methods such as FEM and FVM. In this section, we explain the way to set the boundary condition using the MPS method.

2.4.1. Free surface boundary condition

In the previous studies [34, 58], particle number density is used for judgment of free surface particles. A particle whose particle number density satisfies the following condition is regarded as the free surface particle:

$$n_i < \beta n^0. \tag{16}$$

In this study, we set β as 0.97. Pressure 0 is given to the free surface particle as the boundary condition when the pressure Poisson equation is solved in Eq.(12).

2.4.2. Wall boundary condition

Here, we explain how to express wall boundaries using the MPS method. In order to express wall boundaries in a nozzle as shown in Fig.3, we arrange four layers of particles at the position of wall, as shown in Fig.4. A wall consists

of a double layers of wall particles, with its associated pressure parameter, and a double layers of dummy wall particles, which have no pressure parameter. The dummy wall particles are used only for calculating particle number density of wall particles. Here, to set the Neumann boundary condition for pressure on a wall, as shown in Fig.4, the effective radius r_e for the gradient model is determined so that a dummy wall particle is included within the effective radius when a fluid particle exists near the wall. In calculating the pressure gradient

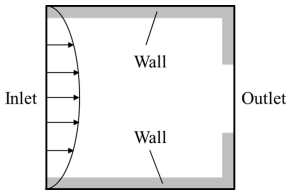

Figure 3: Nozzle

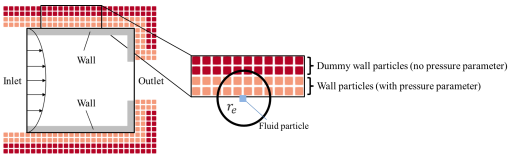

Figure 4: Wall boundary

in Eq.(5) of a fluid particle i near the wall, if a neighboring particle j of the particle i is a dummy wall particle, we do not calculate the pressure gradient of the particle i. This exclusion is equivalent to the fact that the pressure value of a particle i and a particle j is the same, and represents the Neumann boundary condition of pressure gradient 0 on a wall.

In order to impose the no-slip boundary condition on a wall, we use the approximate method where velocities of wall particles are set as 0.

2.4.3. Inlet boundary condition

Eulerian method is using a coordinate system in which coordinates are fixed in the analysis domain. On the other hand, in Lagrangian method like the MPS

method, particles themselves move and coordinates fixed to them are used.

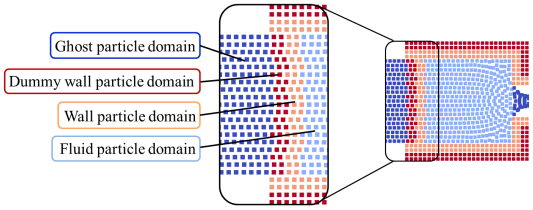

Figure 5: Inlet boundary

The MPS method is a Lagrangian method, and in the inlet of the design domain, we have to make particles flow. In this study, particles are arranged in the left of the inlet at 0s so that particles exist in the inlet when simulation terminates. We impose the initial velocity condition as the Dirichlet boundary condition on them.

To impose the Neumann boundary condition on particles on the inlet, as shown in Fig.5, the domain with $2l_0$ width in the left of the inlet is determined as the wall particle domain (orange squares), where l_0 is the distance between two adjacent particles in the initial configuration, and the domain with $2l_0$ width in the left of the wall particle domain is determined as the dummy wall particle domain (red squares), and the domain with $2l_0$ width in the left of the dummy wall particle domain is determined as the ghost particle domain (blue squares). Here, ghost particles have no parameter. Therefore, as is the case with the wall boundary condition, we impose the Neumann boundary condition of the pressure gradient 0 on the inlet.

2.4.4. Outlet boundary condition

In order to impose the Neumann boundary condition of the velocity on the outlet, fluid particles going out of the outlet are transformed into ghost particles, as shown in Fig.6. In addition, the effective radius for Laplacian model in Eq.(6) is determined so that a ghost particle is included within the radius of the interaction area when a fluid particle exists near the outlet, as

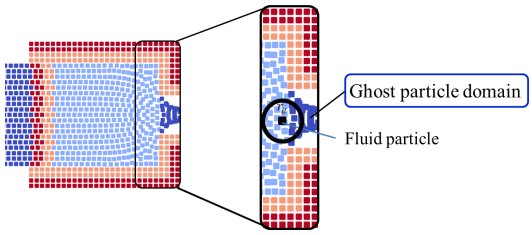

Figure 6: Outlet boundary

shown in Fig.6. Therefore, in calculating the viscous term in Eq.(6) of a fluid particle i near the outlet, if a neighboring particle j of the fluid particle i is a ghost particle, we do not calculate the viscous term of the fluid particle i. This exclusion is equivalent to the fact that the value of a particle i and a particle j have the same value of the velocity, and represents the Neumann boundary condition of the velocity gradient 0 on the outlet.

By transforming fluid particles into ghost particles, the particle number density of fluid particles near the outlet becomes small. For this reason, fluid particles near the outlet are judged as free surface particles, and the pressure of them becomes 0. As the result, this is equivalent to imposing the Dirichlet boundary condition of pressure 0 on the outlet.

3. Topology optimization based on the MPS method

In this section, to construct the topology optimization method using the MPS method incorporating the level set boundary expressions, at first, we explain the concept of topology optimization and level set boundary expressions. Next, we explain the MPS method with level set boundary expressions and we formulate the topology optimization problem using the MPS method. Finally, to derive the sensitivity, we use the adjoint variable method [59].

3.1. Topology optimization method

In the topology optimization, we define the fixed design domain as D, and introduce the following characteristic function χ_Ω, described in the papers of

Murat and Tartar [4]. In other words, we introduce the fixed design domain D including the original design domain Ω. As shown in Fig.7, by utilizing the characteristic function χ_Ω, we replace the original optimization problem with a material distribution problem in the fixed design domain D.

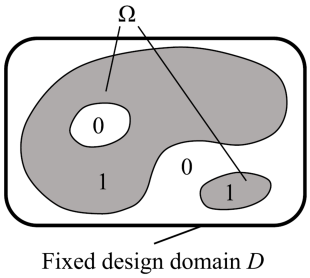

Figure 7: Topology optimization

$$\chi_\Omega(\boldsymbol{x}) = \begin{cases} 1 & \text{if } \boldsymbol{x} \in \Omega \\ 0 & \text{if } \boldsymbol{x} \in D \backslash \Omega \end{cases} . \tag{17}$$

Since the characteristic function allows the optimal solution including partial structures where infinitely small structures are placed at infinitely small intervals, to solve this problem, some regularization or relaxation techniques such as homogenization [60] are introduced. However, in such relaxation technique, the existence of grayscales is allowed in the optimal configurations. On the other hand, the level-set based topology optimization proposed by Yamada et.al [30] is the method of expressing the boundary condition implicitly by utilizing the level set function.

3.2. Level set boundary expressions based on the MPS method

In this study, we consider the fixed design domain D including the void and solid domains Ω shown in Fig.8. In the level set method, the iso-surface of the level set function ϕ implicitly represents the boundary of solid domains. In other words, we represent the structural configurations using the level set function ϕ,

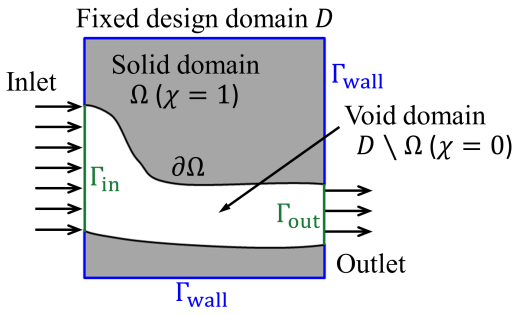

Figure 8: Fixed design domain

where ϕ is positive in solid domains, ϕ is negative in void domains, and ϕ is 0 at boundaries. Since we can arbitrarily set the maximum and minimum of the level set function in boundary expressions using the level set function, in this study, based on the previous study [30], to represent the fictitious interface energy by the level set function added to the objective function, the level set function is constrained to values lying between -1 and 1 in Eq.(18).

$$\begin{cases} 0 < \phi(\boldsymbol{x}) \leq 1 & \text{if } \boldsymbol{x} \in \Omega \\ \phi(\boldsymbol{x}) = 0 & \text{if } \boldsymbol{x} \in \partial\Omega \\ -1 \leq \phi(\boldsymbol{x}) < 0 & \text{if } \boldsymbol{x} \in D \backslash \Omega \end{cases} . \tag{18}$$

Therefore, the characteristic function χ is defined as follows using the level set function:

$$\chi(\phi) = \begin{cases} 1 & \text{if } \quad 0 \leq \phi(\boldsymbol{x}) \\ 0 & \text{if } \quad \phi(\boldsymbol{x}) < 0 \end{cases} . \tag{19}$$

In this study, as shown in Fig.9, a level set function is set on each lattice point in the design domain. In addition, as shown in Fig.10, if $0 \leq \phi(\boldsymbol{x})$, a wall particle representing the solid domain is set at that position, and if $\phi(\boldsymbol{x}) < 0$, a ghost particle representing the void is set so that fluid particles can pass through.

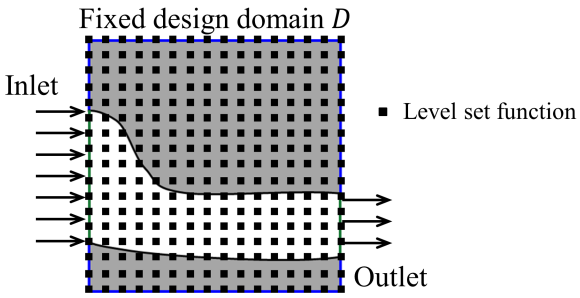

Figure 9: Lattice points where level set functions are set in the design domain

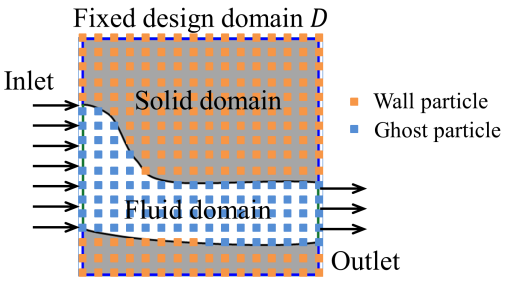

Figure 10: Concept of fixed design domain using the MPS method

3.3. Formulation of optimization problem

In this section, we formulate the optimization problem for the unsteady incompressible flow. In order to perform the sensitivity analysis, the Navier-Stokes equation is represented in the Eulerian coordinate system. Here, we represent implicitly the solid domain in the fixed design domain by using the characteristic function χ as the following equation:

$$\chi(\phi)\boldsymbol{u} = \mathbf{0}. \qquad \text{in } D \tag{20}$$

In this study, since we consider the minimizing of the dissipation of the flow, we can formulate the following optimization problem:

$$\min_{\phi} \quad F(\boldsymbol{u};\phi) = \int_{T_i}^{T_f} \int_{\Omega} \frac{\mu}{2} \left[\nabla \boldsymbol{u} + (\nabla \boldsymbol{u})^T\right] : \left[\nabla \boldsymbol{u} + (\nabla \boldsymbol{u})^T\right] d\Omega dt, \tag{21}$$

$$\text{s.t.} \quad \rho\frac{\partial \boldsymbol{u}}{\partial t} + \rho\left(\boldsymbol{u}\cdot\nabla\right)\boldsymbol{u} - \mu\nabla^2\boldsymbol{u} + \nabla p = \boldsymbol{f}, \qquad \text{in } D\times[T_i,T_f] \tag{22}$$

$$-\nabla\cdot\boldsymbol{u} = 0, \qquad \text{in } D\times[T_i,T_f] \tag{23}$$

$$\chi(\phi)\boldsymbol{u} = \boldsymbol{0}, \qquad \text{in } D\times[T_i,T_f] \tag{24}$$

$$\boldsymbol{u}(T_i,\boldsymbol{x}) = \boldsymbol{u}_0(\boldsymbol{x}), \qquad \text{in } D \tag{25}$$

$$\boldsymbol{u}(t,\boldsymbol{x}) = \boldsymbol{u}_D(t,\boldsymbol{x}), \quad \text{on } (\Gamma_{\text{in}}\cup\Gamma_{\text{wall}})\times[T_i,T_f] \tag{26}$$

$$(-p\boldsymbol{I} + \mu\nabla\boldsymbol{u})\boldsymbol{n} = \boldsymbol{g}, \qquad \text{on } \Gamma_{\text{out}}\times[T_i,T_f] \tag{27}$$

$$G = \int_\Omega \chi(-\phi)d\Omega - V^*V_0 = 0, \tag{28}$$

where μ is the fluid viscosity; $\boldsymbol{u}_0$ is the initial condition of the velocity; $\boldsymbol{u}_D$ and $\boldsymbol{g}$ are the known velocity and stress distribution on Γ_{in} and Γ_{out} as shown in Fig.8 , respectively; $\boldsymbol{n}$ is the unit outward normal vector on $\partial\Omega$; $V^*\in(0,1)$ is the volume fraction of fluid; V_0 is the volume of the fixed design domain D; and $[T_i,T_f]$ is the considered time interval.

3.4. Optimization method

In this study, in order to obtain the optimal solution of the level set function ϕ, we use the following the time evolution equation [30] discretized by the MPS method.

$$\frac{\partial\phi}{\partial t} = -K(J'(\boldsymbol{x}) - \tau\nabla^2\phi), \tag{29}$$

where $J'(\boldsymbol{x})$ is the sensitivity. In solving the Poisson equation of pressure in Eq.(12), the Laplacian model in Eq.(6) is used. In the same way, we discretize Eq.(29) using the Laplacian model in Eq.(6) as follows:

$$\frac{\phi^{k+1}-\phi^k}{\Delta t} = -K(J'(\boldsymbol{x}) - \tau\langle\nabla^2\phi\rangle^{k+1}), \tag{30}$$

In order to obtain the sensitivity, we perform the sensitivity analysis of the optimization problem using the Lagrangian multiplier-based adjoint approach [61, 62], and we treat the volume constraint using the Lagrangian multiplier

based quadratic penalty method [63]. Then, we obtain the adjoint equations of the optimization problem written as follows (see Appendix A for more details):

$$-\rho\frac{\partial \boldsymbol{v}}{\partial t} - \rho\left(\boldsymbol{u}\cdot\nabla\right)\boldsymbol{v} + \rho\left(\nabla\boldsymbol{u}\right)\cdot\boldsymbol{v} - \mu\nabla^2\boldsymbol{v} + \nabla q = -\left(\frac{\partial A}{\partial \boldsymbol{u}} + \nabla\cdot\frac{\partial A}{\partial \nabla\boldsymbol{u}}\right) + \frac{\partial \boldsymbol{f}}{\partial \boldsymbol{u}},$$
$$\text{in } D\times[T_i, T_f] \tag{31}$$
$$-\nabla\cdot\boldsymbol{v} = \frac{\partial A}{\partial p}p + \frac{\partial \boldsymbol{f}}{\partial p}\cdot\boldsymbol{v},$$
$$\text{in } D\times[T_i, T_f] \tag{32}$$
$$\boldsymbol{v}\left(T_f, \boldsymbol{x}\right) = \boldsymbol{0},$$
$$\text{in } D \tag{33}$$
$$\boldsymbol{v} = \boldsymbol{0},$$
$$\text{on } \left(\Gamma_{\text{in}}\cup\Gamma_{\text{wall}}\right)\times[T_i, T_f] \tag{34}$$
$$\left(-q\boldsymbol{I} + \mu\nabla\boldsymbol{v}\right)\boldsymbol{n} = -\rho\left(\boldsymbol{u}\cdot\boldsymbol{n}\right)\boldsymbol{v} - \frac{\partial A}{\partial \nabla\boldsymbol{u}}\boldsymbol{n},$$
$$\text{on } \Gamma_{\text{out}}\times[T_i, T_f] \tag{35}$$

where $\boldsymbol{v}$ and q are the adjoint variables of the fluid velocity $\boldsymbol{u}$ and pressure p, respectively; and A is the dissipation of the flow [12, 64] as follows:

$$A = \frac{\mu}{2}\left[\nabla\boldsymbol{u} + \left(\nabla\boldsymbol{u}\right)^T\right] : \left[\nabla\boldsymbol{u} + \left(\nabla\boldsymbol{u}\right)^T\right]. \tag{36}$$

Here, each term is expressed as follows:

$$\frac{\partial A}{\partial \boldsymbol{u}} = 0, \tag{37}$$
$$\nabla\cdot\frac{\partial A}{\partial \nabla\boldsymbol{u}} = 2\mu\nabla^2\boldsymbol{u}, \tag{38}$$
$$\frac{\partial A}{\partial p}p = 0. \tag{39}$$

The design sensitivity also is obtained as follows (see Appendix A for more details):

$$J'(\boldsymbol{x}) = \int_{T_i}^{T_f}\boldsymbol{u}\cdot\boldsymbol{v}dt + \lambda - \Lambda G, \tag{40}$$

where, λ and Λ are the Lagrangian multiplier and penalty parameter, respectively.

3.5. Discretization of the adjoint equation

Here, we explain how to discretize the adjoint equation (31) obtained by sensitivity analysis using the MPS method. Eq.(31) is expressed in the Eulerian coordinate system as a result of performing sensitivity analysis, but the MPS method is a Lagrangian method. Therefore, it is necessary to rewrite Eq.(31) from a Eulerian coordinate system to a Lagrangian coordinate system. We transform Eq.(31) as follows:

$$\frac{\partial \boldsymbol{v}}{\partial t} + (\boldsymbol{u} \cdot \nabla)\, \boldsymbol{v} = -\nu \nabla^2 \boldsymbol{v} + (\nabla \boldsymbol{u}) \cdot \boldsymbol{v} + 2\nu \nabla^2 \boldsymbol{u} - \frac{1}{\rho} \frac{\partial \boldsymbol{f}}{\partial \boldsymbol{u}} + \frac{1}{\rho} \nabla q. \tag{41}$$

Here, we regard the item $-\nu \nabla^2 \boldsymbol{v}$ as a viscosity term, the item $\frac{1}{\rho} \nabla q$ as a pressure term, and the other terms of the right side of Eq.(41) as external force terms. Regarding the item $(\boldsymbol{u} \cdot \nabla)\, \boldsymbol{v}$, considering the relation of the Lagrangian coordinate system to the Eulerian coordinate system, it becomes as follows:

$$\frac{D\boldsymbol{v}}{Dt} = \frac{\partial \boldsymbol{v}}{\partial t} + \frac{\partial \boldsymbol{v}}{\partial \boldsymbol{x}} \frac{\partial \boldsymbol{x}}{\partial t} = \frac{\partial \boldsymbol{v}}{\partial t} + (\boldsymbol{v} \cdot \nabla)\, \boldsymbol{v}, \tag{42}$$

where $\boldsymbol{x}$ is position vector in the adjoint equation. Therefore, comparing the left side of Eq.(41) and Eq.(42), we use the velocity $\boldsymbol{u}$ for moving particles in the adjoint equation. In this study, the left side of Eq.(41) is represented as follows:

$$\frac{D_u \boldsymbol{v}}{D_u t} = \frac{\partial \boldsymbol{v}}{\partial t} + (\boldsymbol{u} \cdot \nabla)\, \boldsymbol{v}. \tag{43}$$

To summarize the above, the adjoint equation is represented as follows:

$$\frac{D_u \boldsymbol{v}}{D_u t} = -\nu \nabla^2 \boldsymbol{v} + (\nabla \boldsymbol{u}) \cdot \boldsymbol{v} + 2\nu \nabla^2 \boldsymbol{u} - \frac{1}{\rho} \frac{\partial \boldsymbol{f}}{\partial \boldsymbol{u}} + \frac{1}{\rho} \nabla q. \tag{44}$$

The MPS method employs the fractional step algorithm where a one-time step is divided into two processes. We divide Eq.(44) into two parts as follows:

$$\frac{\boldsymbol{v}_i^* - \boldsymbol{v}_i^{k+1}}{\Delta t} = -\nu \nabla^2 \boldsymbol{v} + (\nabla \boldsymbol{u}) \cdot \boldsymbol{v} + 2\nu \nabla^2 \boldsymbol{u} - \frac{1}{\rho} \frac{\partial \boldsymbol{f}}{\partial \boldsymbol{u}}, \tag{45}$$

$$\frac{\boldsymbol{v}_i^k - \boldsymbol{v}_i^*}{\Delta t} = \frac{1}{\rho} \nabla q. \tag{46}$$

The way of solving after this is the same as how to solve the governing equation.

4. Numerical implementation

In this section, to obtain the optimal configuration using the MPS method, at first, we explain the optimization algorithm. Next, we discuss the numerical implementation method.

4.1. Optimization algorithm

In this study, the optimization algorithm of the proposed method is as follows:

(1) Level set functions are initialized and the initial values of the Lagrangian multiplier λ_0 and penalty parameter Λ_0 are chosen based on numerical experiments.

(2) The velocity $\boldsymbol{u}$ and the pressure p are obtained by solving the governing equation using the MPS method.

(3) The objective function is calculated.

(4) If the criteria of the objective function and volume constraint are satisfied, an optimal configuration is obtained and the optimization is finished, otherwise, the adjoint variables $\boldsymbol{v}$ and q are obtained by solving the adjoint equations using the MPS method.

(5) The design sensitivity is calculated.

(6) The level set function is evolved by solving Eq.(29). The Lagrangian multiplier λ and penalty parameter Λ are updated as [63] [65]

$$\lambda_k = \lambda_{k-1} G, \tag{47}$$

$$\Lambda_k = \frac{1}{\alpha}\Lambda_{k-1}, \tag{48}$$

where α is chosen to be 0.9 in this paper.

(7) The optimization procedure returns to the second step.

4.2. Numerical implementation using the MPS method

4.2.1. Interpolation of velocity using MPS method

In this study, as shown in Fig.9, we set the level set function on the lattice points in the design domain. Here, the velocity in the objective function and

sensitivity is used for the velocity on the lattice points where level set functions are set. However, the MPS method is a Lagrangian method, and fluid particles do not always exist on the lattice points where level set functions are set. In this study, in order to interpolate the velocity of the lattice points, we define the following velocities of the lattice points, and obtain the velocity on the lattice points where level set functions are set:

$$\boldsymbol{u}_k = \frac{\sum_j \boldsymbol{u}_j w(|\boldsymbol{r}_j - \boldsymbol{r}_k|)}{\sum_j w(|\boldsymbol{r}_j - \boldsymbol{r}_k|)}, \tag{49}$$

$$\boldsymbol{v}_k = \frac{\sum_j \boldsymbol{v}_j w(|\boldsymbol{r}_j - \boldsymbol{r}_k|)}{\sum_j w(|\boldsymbol{r}_j - \boldsymbol{r}_k|)}. \tag{50}$$

4.2.2. Local-in-time method

In order to obtain the design sensitivity J' in Eq.(40), the velocity $\boldsymbol{u}$ and the adjoint velocity $\boldsymbol{v}$ at each time on the lattice points where level set functions are set are necessary. In a conventional method for solving unsteady design optimization problems, the global-in-time (GT) method is used as shown in Fig.11. When the adjoint equation is analyzed using the GT method, firstly, we analyze the governing equation in the $+\Delta t$ direction from T_i to T_f over the entire time interval. Then, we obtain the velocity $\boldsymbol{u}$ on the lattice points where level set functions are set by interpolating the velocity there using Eq. (49). Next, we analyze the adjoint equation in the $-\Delta t$ direction from T_f to T_i over the entire time interval. Here, the velocity of the particle existing at the position and time k in the governing equation need to be used for the velocities $\boldsymbol{u}$ in the adjoint equation at the same position and time k. However, since the MPS method is a Lagrangian method, particles do not always exist at the position. Therefore, it is necessary to interpolate the velocities in the governing equation at the position and time k using the velocity on the lattice points where level set functions are set. In other words, when analyzing the adjoint equation, all the velocities over the entire time interval on the lattice points where level set functions are set must be saved, which makes the memory cost become enormous.

Therefore, in this study, we employ the local-in-time (LT) method [66]. The

basic idea of the LT method is dividing the entire time interval into several subintervals, calculating the governing and adjoint equations in each subinterval, and approximating the global objective function and sensitivity as a combination of local derivatives computed for each time subinterval, as shown in Fig.12. In other words, The LT is analyzing the governing and adjoint equations in the $(T_f - T_i)/\Delta t$ subsections from T_i to T_f over the entire time interval. Therefore, first, the velocity $\boldsymbol{u}$ at time k is obtained for each particle. Then, the adjoint equation is analyzed using it for each particle. Thereafter, this process is repeated until the end time T_f. By doing it like this, only the velocity $\boldsymbol{u}$ in the governing equation at time k is needed to analyze the adjoint equation at time k without interpolating the velocities and saving them over the entire time interval. Then, the approximate design sensitivity can be obtained by calculating the design sensitivity for each time subinterval and adding them over the entire time interval. Therefore, it is unnecessary to save the velocities in the governing equation over the entire time interval like the GT method, and the memory cost can be drastically reduced.

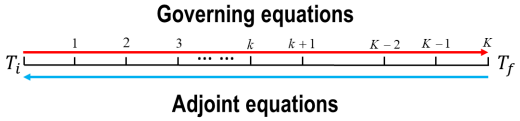

Figure 11: A sketch of the algorithm using the global-in-time method

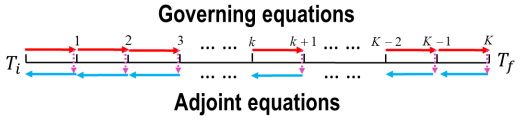

Figure 12: A sketch of the algorithm using the local-in-time method

5. Numerical examples

In this section, several numerical examples are presented for the optimization using the MPS method, and we demonstrate the validity and the availability of the proposed method. All numerical examples use the same parameters: $\rho = 1.0$, $\tau = 1.0 \times 10^{-4}$, and $K = 1$. Each level set function is initialized to -1.0 so that the initial configuration is set to be a void that allows fluid particles to pass through. In addition, in the following numerical examples, the no-slip boundary condition is Dirichlet type, where $\boldsymbol{u}_D$ is set as 0; the open boundary condition is Neumann type, where $\boldsymbol{g}$ is set as 0. In order to implicitly represent structural configurations using the iso-surface of the level set function, all optimal configurations are exhibited by showing the iso-surface of $\phi = 0$. Here, we interpolate the iso-surface of $\phi = 0$ using the fourth order polynomial.

5.1. A nozzle design problem

5.1.1. Validity of the proposed method

First, we demonstrate the validity of the proposed optimization method by comparing an obtained result using the MPS method with the result using the finite element method in the previous study [31]. The design settings for the nozzle design problem are shown in Fig.13.

The fluid velocity at the inlet is given in the form of parabola shown in Fig.13 using the representative velocity $U_0 = 1.0$, which is the maximum velocity at the inlet. This inlet velocity is maximum at the center of the inlet and 0 at walls of both sides of the inlet. The pressure at the outlet is set as $p_0 = 0$. The volume constraint $V^* = 0.60$, the average particle distance $l_0 = 0.050$, and Reynolds number is represented as $\mathrm{Re} = U_0 L_0/\nu = 10$, where we define the characteristic length L_0 as the width of the inlet. The calculation conditions are shown in Table 1. Here, as a benchmark problem, we deal with a a well known steady state problem in the FEM and the initial configuration is a state where the fixed design domain is filled with fluid. On the other hand, the MPS

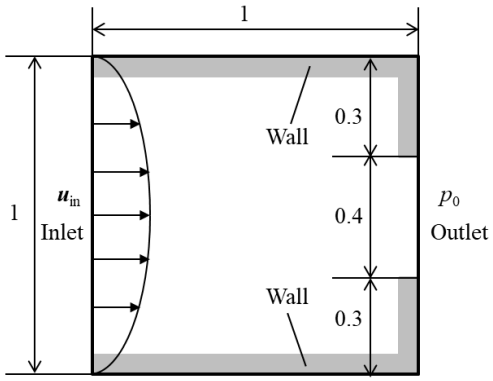

Figure 13: Design settings

Parameter	Value
Effective radius (r_e) for particle number density	$2.1l_0$ (m)
Effective radius (r_e) for gradient	$2.1l_0$ (m)
Effective radius (r_e) for Laplacian	$3.1l_0$ (m)
Initial values of Lagrangian multiplier (λ_0)	-10.0
Initial values of penalty parameter (Λ_0)	10.0
Initial time (T_i)	2.5(s)
Final time (T_f)	4.0(s)

Table 1: Calculation condition for nozzle design problem

method is an analysis method of unsteady flow. In order to match the initial condition of the optimization process in the proposed method with the FEM, the optimization process using the proposed method starts from the state where the flow is constant and the fixed design domain is filled with fluid particles.

Fig.14 shows the movement of fluid particles from 0s to 4s in the nozzle model. Fig.15 shows the convergence history of configurations and Fig.16 shows the optimal configurations based on the MPS method and FEM approaches for the nozzle design problem. Comparing the result using the proposed method and the FEM in Fig.16, optimal configurations are slightly different in the inlet.

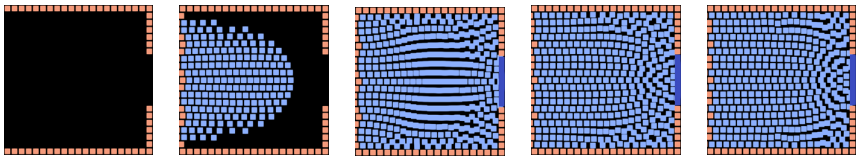

(a) $t = 0.0$(s) (b) $t = 1.0$(s) (c) $t = 2.0$(s) (d) $t = 3.0$(s) (e) $t = 4.0$(s)

Figure 14: Fluid particles movement

This is because in the proposed method, values of level set functions on the inlet are fixed to -1 so that the inlet is not blocked by wall particles. This enables fluid particles to flow into the inlet. Therefore, in the optimal configuration obtained by the proposed method, there is no wall particle representing the solid domain in the inlet. General similarity can be confirmed to the results based on the proposed method and FEM except for the inlet and we can demonstrate the validity of the proposed method.

5.1.2. Dependency of optimal configurations on average particle distance l_0

Next, we investigate the dependency of the optimal configurations with respect to the average particle distance l_0. Here, we compare two cases using average particle distance of $l_0 = 0.050$ and $l_0 = 0.025$ under the same volume constraint. Also, the Reynolds number is set as $\mathrm{Re} = 10$ in order to ensure that the Reynolds number condition is the same in both cases where the average particle distance l_0 is different.

From Fig.17, both results have the similar optimal configurations so that it is indicated that the dependency of optimal configurations on the average particle distance is low.

5.2. A bend pipe design problem

Second, we examine the dependency of the optimal configuration on the Reynolds number, using the objective function F in Eq. (21). Fig.18 shows the design settings for the bend pipe design problem. The fluid velocity at the inlet is given in the form of parabola shown in Fig.18 using the representative

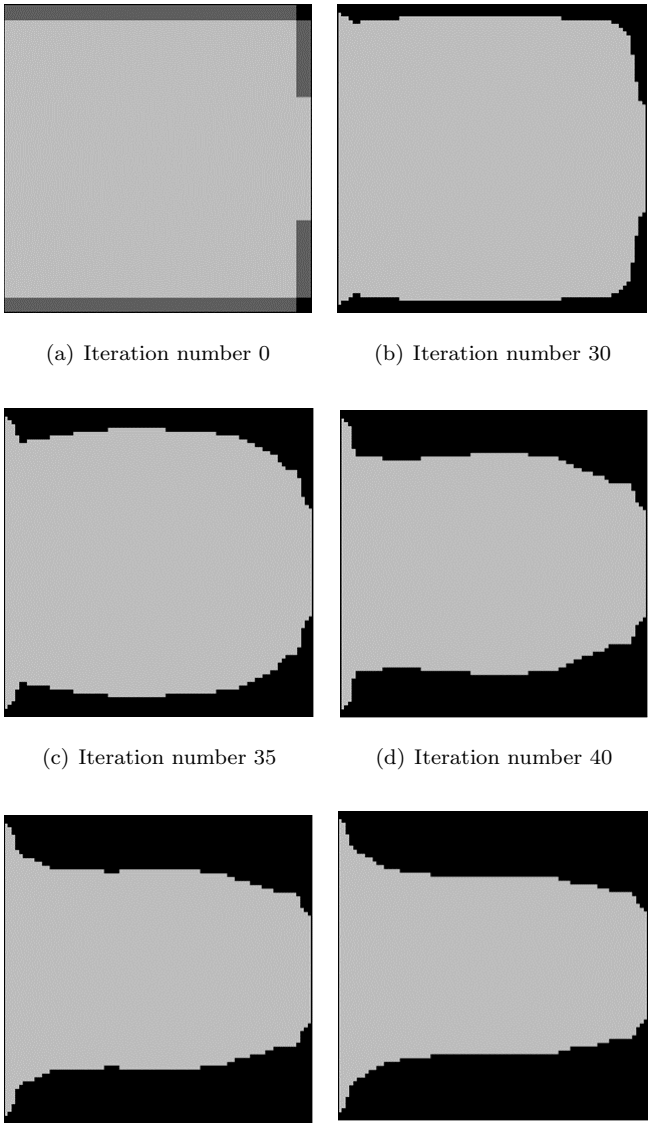

(a) Iteration number 0

(b) Iteration number 30

(c) Iteration number 35

(d) Iteration number 40

(e) Iteration number 60

(f) Iteration number 75 (Optimal configuration)

Figure 15: Optimization histories and optimal configuration

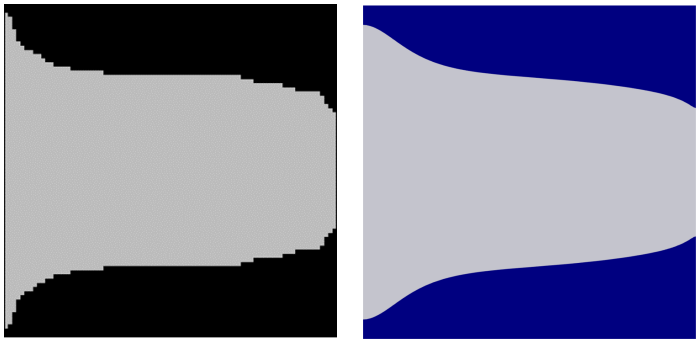

(a) MPS method (b) FEM

Figure 16: Comparison of MPS method and FEM results

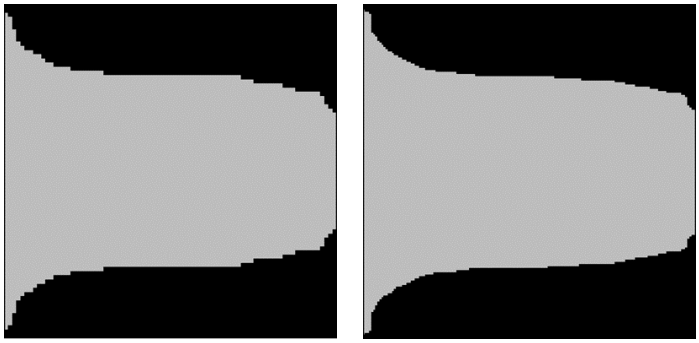

(a) $l_0 = 0.050$ (b) $l_0 = 0.025$

Figure 17: Dependency of optimal configurations on average particle distance

velocity $U_0 = 1.0$, which is the maximum velocity at the inlet. This inlet velocity is maximum at the center of the inlet and 0 at walls of both sides of the inlet. The pressure at the outlet is set as $p_0 = 0$. The volume constraint $V^* = 0.35$, and the average particle distance $l_0 = 0.025$. The calculation conditions are shown in Table 2. Here, we compare two cases using the Reynolds numbers of Re = 10 and Re = 100. In order to start the optimization process after becoming a state that can be regarded as steady state, the optimization process starts from the state where the design region is filled with fluid particles.

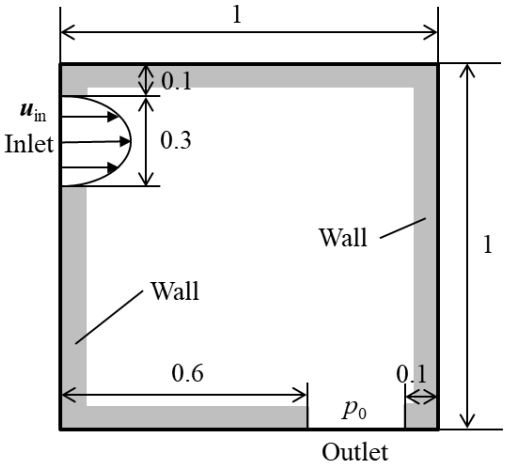

Figure 18: Design settings

Figs.19 and 20 show the movement of fluid particles from 0s to 7s of Re = 1 and from 0s to 12s of Re = 100 in the bend pipe model, respectively. From Fig.21, the differences in the optimal configurations indicate that the value of the Reynolds number affects the optimal configurations. As the Reynolds number is increased, the radius of curvature is decreased. This dependency of the optimal configuration on Reynolds number is consistent with previous studies [31].

Parameter	Value
Effective radius (r_e) for particle number density (Re = 1)	$4.2l_0$ (m)
Effective radius (r_e) for gradient (Re = 1)	$4.2l_0$ (m)
Effective radius (r_e) for Laplacian (Re = 1)	$6.3l_0$ (m)
Effective radius (r_e) for particle number density (Re = 100)	$3.15l_0$ (m)
Effective radius (r_e) for gradient (Re = 100)	$3.15l_0$ (m)
Effective radius (r_e) for Laplacian (Re = 100)	$4.65l_0$ (m)
Initial values of Lagrangian multiplier (λ_0)	-1.0
Initial values of penalty parameter (Λ_0)	1.0
Initial time (T_i) for (Re = 1)	6.0(s)
Final time (T_f) for (Re = 1)	7.0(s)
Initial time (T_i) for (Re = 100)	11.0(s)
Final time (T_f) for (Re = 100)	12.0(s)

Table 2: Calculation condition for bend pipe design problem

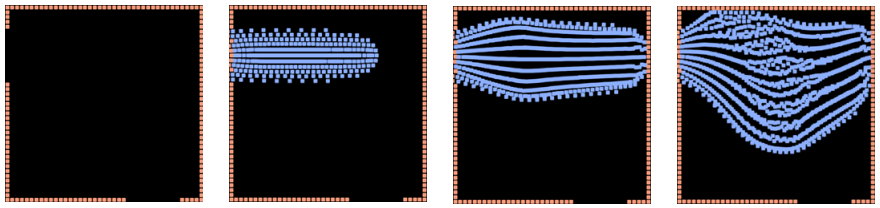

(a) $t = 0.0$(s) (b) $t = 1.0$(s) (c) $t = 2.0$(s) (d) $t = 3.0$(s)

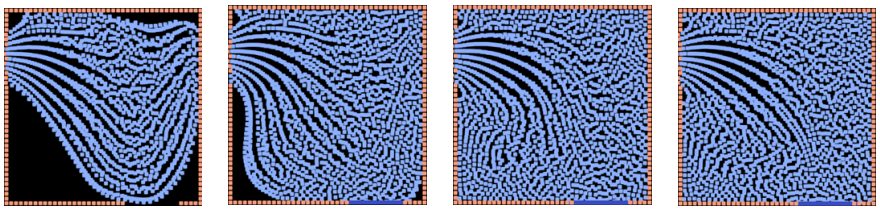

(e) $t = 4.0$(s) (f) $t = 5.0$(s) (g) $t = 6.0$(s) (h) $t = 7.0$(s)

Figure 19: Fluid particles movement of Re = 1

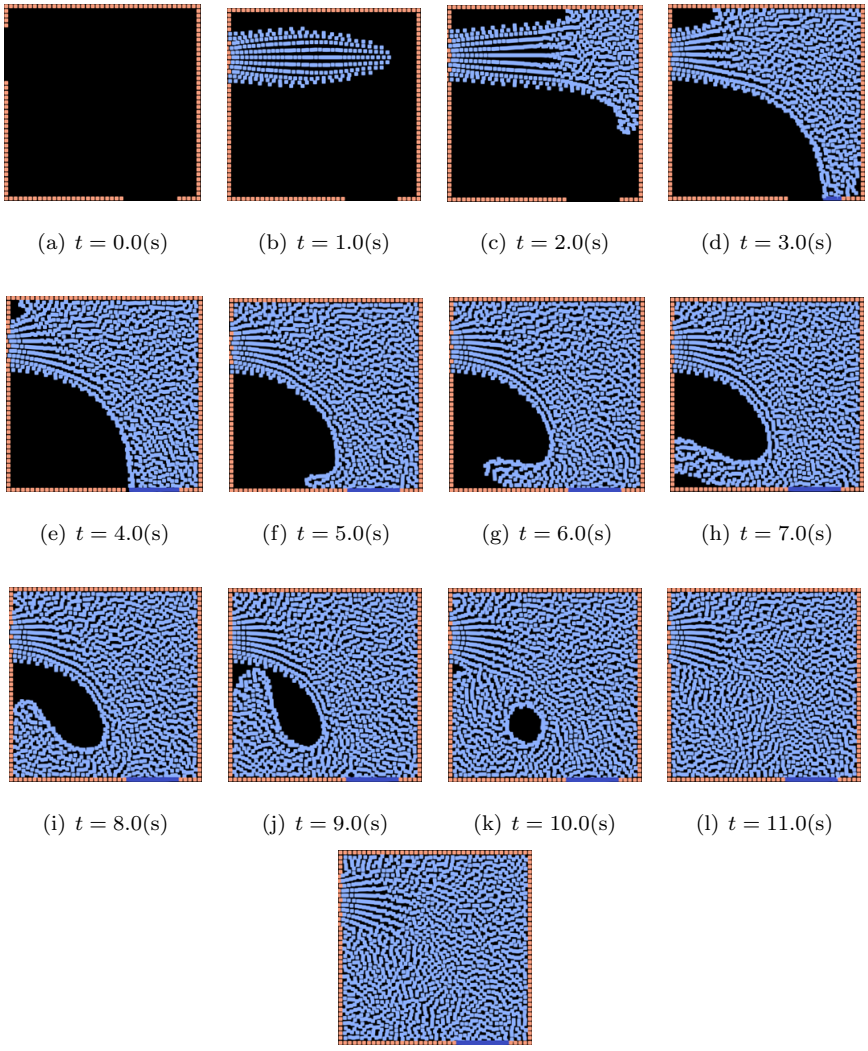

(a) $t = 0.0$(s) (b) $t = 1.0$(s) (c) $t = 2.0$(s) (d) $t = 3.0$(s)

(e) $t = 4.0$(s) (f) $t = 5.0$(s) (g) $t = 6.0$(s) (h) $t = 7.0$(s)

(i) $t = 8.0$(s) (j) $t = 9.0$(s) (k) $t = 10.0$(s) (l) $t = 11.0$(s)

(m) $t = 12.0$(s)

Figure 20: Fluid particles movement of Re = 100

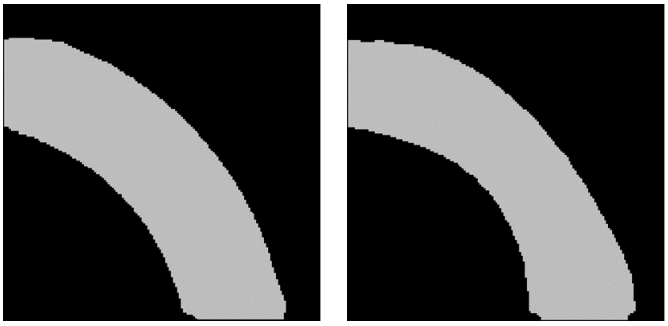

(a) Re = 1 (b) Re = 100

Figure 21: Dependency of optimal configurations on Reynolds number

5.3. A double pipe design problem

A double pipe is designed in this numerical example, using the objective function F in Eq.(21). The design settings are shown in Figs.22(a) and 22(b). The fluid velocity at the inlet is given in the form of parabola shown in Figs.22(a) and 22(b) using the representative velocity $U_0 = 1.0$, which is the maximum velocity at the inlet. This inlet velocity is maximum at the center of the inlet and 0 at walls of both sides of the inlet. The pressure at the outlet is set as $p_0 = 0$. The volume constraint $V^* = 0.40$, the average particle distance $l_0 = 0.025$, and Reynolds number Re $= 1$. The calculation conditions are shown in Table 3. Here, we compare two cases using the distance between the two inlets and two outlets of $w = 1/5$ and $w = 1/20$. In order to start the optimization process after becoming a state that can be regarded as steady state, the optimization process starts from the state where the design domain is filled with fluid particles. From Figs.23(a) and 23(b), the differences in the optimal configurations indicate that the length of the distance between the two inlets and two outlets affects the optimal configurations. From Fig.23(a), two straight channels are formed, whereas from Fig.23(b), two channels are connected into one and then branch into two. Here, the friction with the wall (the contact area with the wall) and the loss of inertial force can be considered as factors of the dissipation of the flow. In $w = 1/5$ (Fig.23(a)), to minimize energy loss, the

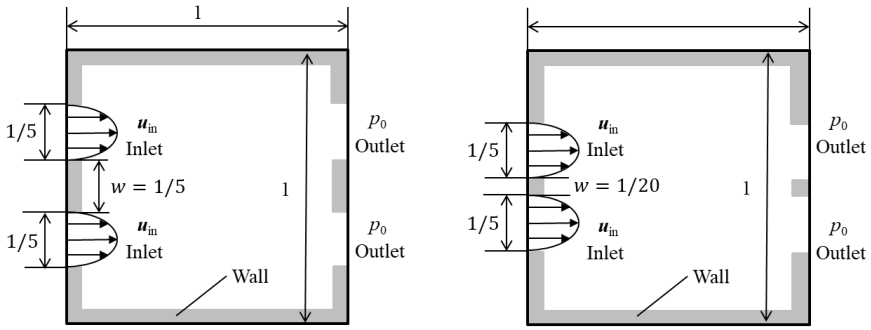

(a) $w = 1/5$ (b) $w = 1/20$

Figure 22: Design settings

Parameter	Value
Effective radius (r_e) for particle number density	$4.1l_0$ (m)
Effective radius (r_e) for gradient	$4.1l_0$ (m)
Effective radius (r_e) for Laplacian	$6.1l_0$ (m)
Initial values of Lagrangian multiplier (λ_0)	-1.0
Initial values of penalty parameter (Λ_0)	1.0
Initial time (T_i)	5.0(s)
Final time (T_f)	6.0(s)

Table 3: Calculation condition for double pipe design problem

linear channel is obtained because the effect of suppressing loss of inertial force is dominant over that of making the contact area with the wall smaller. On the other hand, in $w = 1/20$ (Fig.23(b)), connecting two channels into one is because the effect of making the contact area with the wall smaller is dominant over that of suppressing loss of inertial force.

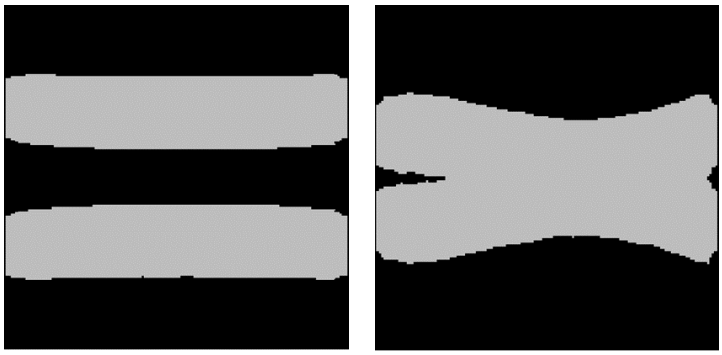

(a) $w = 1/5$ (b) $w = 1/20$

Figure 23: Optimal configurations

5.4. A free surface flow problem

Finally, we apply the proposed method to a free surface flow problem, using the objective function F in Eq.(21). Fig.24 shows the design settings for a free surface flow problem. The fluid velocity at the inlet is given in the form of parabola shown in Fig.24 using the representative velocity U_0, which is the maximum velocity at the inlet. This inlet velocity is maximum at the free surface of the inlet and 0 at the bottom wall of the inlet. The pressure at the outlet is set as $p_0 = 0$. The volume constraint $V^* = 0.65$, and the average particle distance $l_0 = 0.025$. In this case, we set the gravity $\boldsymbol{g} = -9.8$. The calculation conditions are shown in Table 4. In this case, the optimization process starts after becoming a state that can be regarded as steady state. Here, we compare two cases using the inlet velocities of $U_0 = 1.0$ and $U_0 = 2.0$. Figs.25 and 26 show the initial configuration and fluid flow at 3.0s in the initial configuration, using the inlet velocities of $U_0 = 1.0$ and $U_0 = 2.0$, respectively. In Figs.25 and

26, orange and blue particles are wall and ghost particles on the lattice points where level set functions are set in the fixed design domain, respectively, as described above in Section 3.2. The light blue particles are fluid particles. The upper black domain in each figure represents a void which is non-design domain. Figs.27(a) and 27(b) show the optimal configuration of $U_0 = 1.0$ and $U_0 = 2.0$, respectively, where black is solid, gray is void in the fixed design domain and white represents void in the non-design domain. In addition, Table 5 shows the values of the objective function F under each condition.

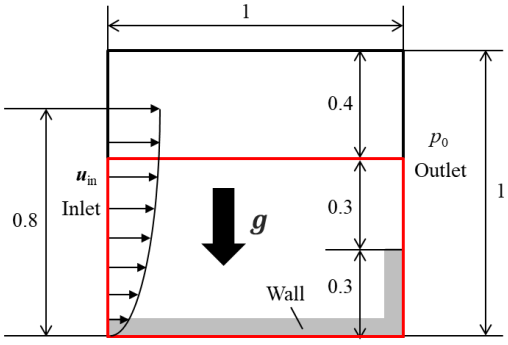

Figure 24: Design settings

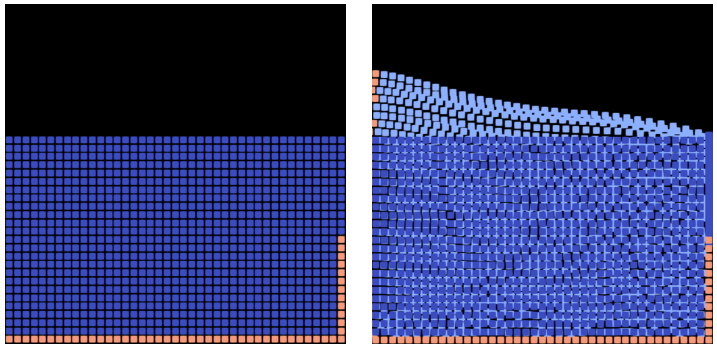

(a) Initial configuration

(b) Fluid flow at 3.0s in the initial configuration

Figure 25: $U_0 = 1.0$

Parameter	Value
Effective radius (r_e) for particle number density	$2.1l_0$ (m)
Effective radius (r_e) for gradient	$2.1l_0$ (m)
Effective radius (r_e) for Laplacian	$3.1l_0$ (m)
Initial values of Lagrangian multiplier (λ_0) for $U_0 = 1.0$	-1.8
Initial values of penalty parameter (Λ_0) for $U_0 = 1.0$	1.8
Initial values of Lagrangian multiplier (λ_0) for $U_0 = 2.0$	-3.0
Initial values of penalty parameter (Λ_0) for $U_0 = 2.0$	3.0
Initial time (T_i) for $U_0 = 1.0$	3.0(s)
Final time (T_f) for $U_0 = 1.0$	4.0(s)
Initial time (T_i) for $U_0 = 2.0$	2.0(s)
Final time (T_f) for $U_0 = 2.0$	3.0(s)

Table 4: Calculation condition for free surface flow problem

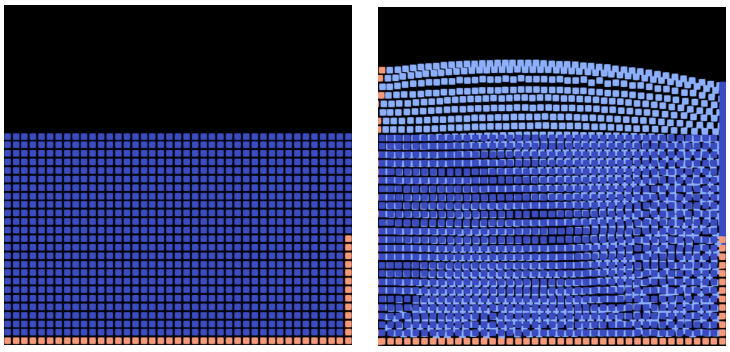

(a) Initial configuration

(b) Fluid flow at 3.0s in the initial configuration

Figure 26: $U_0 = 2.0$

The value of F	Analysis condition for $U_0 = 1.0$	Analysis condition for $U_0 = 2.0$
Optimal configuration for $U_0 = 1.0$	$\mathbf{2.69 \times 10^6}$	5.84×10^6
Optimal configuration for $U_0 = 2.0$	2.73×10^6	$\mathbf{5.82 \times 10^6}$

Table 5: Comparison of the values of objective function F

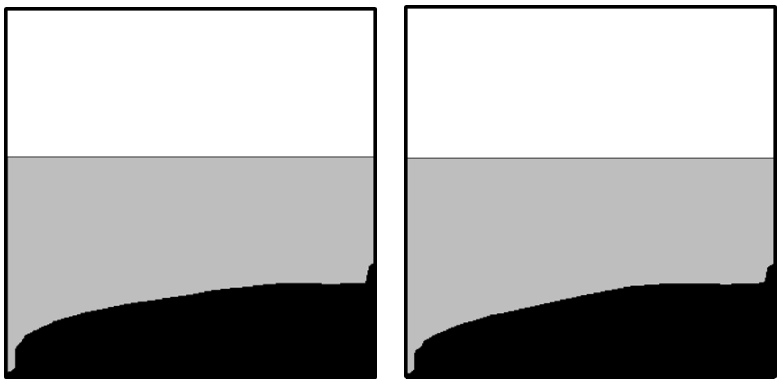

(a) $U_0 = 1.0$ (b) $U_0 = 2.0$

Figure 27: Optimal configurations

From Figs.27(a) and 27(b), the differences in the optimal configurations confirm that the value of the inlet velocity affects the optimal configurations. From Table 5 , under the analysis condition for $U_0 = 1.0$, the objective function of optimal configuration for $U_0 = 1.0$ is smaller than that for $U_0 = 2.0$. Under analysis condition for $U_0 = 2.0$, the objective function of optimal configuration for $U_0 = 2.0$ is smaller than that for $U_0 = 1.0$. Also, from the optimal configurations shown in Figs.27(a) and 27(b), we can see that obstacles are bulging towards the outlet. This structural feature raises the fluid and it is found that the speed and hence the pressure loss is minimized. Therefore, it is indicated that optimal configurations are valid physically and intuitively.

6. Conclusion

In this paper, a new topology optimization method for fluid dynamics problems has been achieved using the MPS method. We achieved the following:

(1) A topology optimization problem was formulated using the MPS method, where the objective function for minimizing the energy dissipation of the flow was set.

(2) To obtain an optimal configuration, based on the formulation of the topology optimization problem, the sensitivity analysis was performed using the Lagrangian multiplier-based adjoint approach in the Eulerian coordinate system, and the optimization algorithm was constructed. To discretize and implement the adjoint equations using the MPS method, the adjoint equations were rewritten from the Eulerian coordinate system to the Lagrangian coordinate system.

(3) Several numerical examples were presented to demonstrate the validity and the availability of the proposed method. From the numerical example of a nozzle design problem, we confirmed that the optimal configuration obtained using the MPS method has the same topology with the result using FEM. It also considered that the proposed method shows low dependency on the average particle distance because we obtained physically reasonable configurations with the same tendency as in previous studies. From a bend pipe design problem, we demonstrated that the optimal configuration obtained using the proposed method shows dependency on the Reynolds number. Finally, from a free surface flow problem, it is indicated that the proposed method can derive a valid optimal configuration in the case which includes free surface flows.

(4) In this paper, we have constructed a topology optimization method based on the MPS method as a basic methodology. Yamada et al.[67] has proposed a particle method using a fully explicit method suitable for parallelization calculation. Based on this study and the proposed method, it is considered easy to extend to the topology optimization method using the explicit method only by changing the way to analyze adjoint equations. The explicit method performed by parallel computation allows expansion to more complicated problems and 3D problems. Therefore, this paper, which is the basis, is considered to be meaningful.

Appendix A. Derivation of the adjoint equations and sensitivity

Here, we discuss the details concerning the derivation of the adjoint equations. The weak form of the Navier-Stokes equations is as follows:

$$
\begin{aligned}
e(\boldsymbol{u},p;\phi) = & \int_{T_i}^{T_f}\int_{\Omega}\left[\rho\frac{\partial \boldsymbol{u}}{\partial t}+\rho\left(\boldsymbol{u}\cdot\nabla\right)\boldsymbol{u}-\mu\nabla^2\boldsymbol{u}+\nabla p-\boldsymbol{f}\right]\cdot\boldsymbol{v}\ d\Omega dt \\
& +\int_{T_i}^{T_f}\int_{\Omega} q\ (-\nabla\cdot\boldsymbol{u})\ d\Omega dt+\int_{T_i}^{T_f}\int_{\Omega}\chi(\phi)\boldsymbol{u}\cdot\boldsymbol{v}\ d\Omega dt+\int_{\Omega}(\boldsymbol{u}\cdot\boldsymbol{v})|_{t=T_i}\ d\Omega \\
& +\int_{T_i}^{T_f}\int_{\Gamma_{\text{in}}\cup\Gamma_{\text{wall}}}\boldsymbol{u}\cdot\boldsymbol{v}\ d\Gamma dt+\int_{T_i}^{T_f}\int_{\Gamma_{\text{out}}}(-p\boldsymbol{I}+\mu\nabla\boldsymbol{u})\boldsymbol{n}\cdot\boldsymbol{v}\ d\Gamma dt \\
= & \rho\int_{\Omega}\int_{T_i}^{T_f}\left[\frac{\partial(\boldsymbol{u}\cdot\boldsymbol{v})}{\partial t}-\boldsymbol{u}\cdot\frac{\partial\boldsymbol{v}}{\partial t}\right]dtd\Omega+\rho\int_{T_i}^{T_f}\int_{\Omega}\left(\boldsymbol{u}\cdot\nabla\right)\boldsymbol{u}\cdot\boldsymbol{v}dtd\Omega \\
& +\mu\int_{T_i}^{T_f}\int_{\Omega}\left[\nabla\boldsymbol{u}\colon\nabla\boldsymbol{v}-\nabla\cdot(\nabla\boldsymbol{u}\cdot\boldsymbol{v})\right]d\Omega dt-\int_{T_i}^{T_f}\int_{\Omega}\boldsymbol{f}\cdot\boldsymbol{v}\ d\Omega dt-\int_{T_i}^{T_f}\int_{\Omega}q\nabla\cdot\boldsymbol{u}\ d\Omega dt \\
& +\int_{T_i}^{T_f}\int_{\Omega}\chi(\phi)\boldsymbol{u}\cdot\boldsymbol{v}\ d\Omega dt+\int_{\Omega}(\boldsymbol{u}\cdot\boldsymbol{v})|_{t=T_i}\ d\Omega+\int_{T_i}^{T_f}\int_{\Gamma_{\text{in}}\cup\Gamma_{\text{wall}}}\boldsymbol{u}\cdot\boldsymbol{v}\ d\Gamma dt \\
& +\int_{T_i}^{T_f}\int_{\Gamma_{\text{out}}}(-p\boldsymbol{I}+\mu\nabla\boldsymbol{u})\boldsymbol{n}\cdot\boldsymbol{v}\ d\Gamma dt \\
= & \rho\int_{\Omega}[(\boldsymbol{u}\cdot\boldsymbol{v})|_{t=T_f}-(\boldsymbol{u}\cdot\boldsymbol{v})|_{t=T_i}]d\Omega-\rho\int_{T_i}^{T_f}\int_{\Omega}\boldsymbol{u}\cdot\frac{\partial\boldsymbol{v}}{\partial t}\ d\Omega dt \\
& +\rho\int_{T_i}^{T_f}\int_{\Omega}\left(\boldsymbol{u}\cdot\nabla\right)\boldsymbol{u}\cdot\boldsymbol{v}d\Omega dt+\mu\int_{T_i}^{T_f}\int_{\Omega}\nabla\boldsymbol{u}\colon\nabla\boldsymbol{v}\ d\Omega dt-\int_{T_i}^{T_f}\int_{\Omega}p\nabla\cdot\boldsymbol{v}\ d\Omega dt \\
& -\int_{T_i}^{T_f}\int_{\Omega}\boldsymbol{f}\cdot\boldsymbol{v}\ d\Omega dt+\int_{T_i}^{T_f}\int_{\partial\Omega}[(p\boldsymbol{I}-\mu\nabla\boldsymbol{u})\boldsymbol{n}\cdot\boldsymbol{v}]|_{\boldsymbol{u}=\boldsymbol{u}_D}\ d\Gamma dt \\
& -\int_{T_i}^{T_f}\int_{\Omega}q\nabla\cdot\boldsymbol{u}\ d\Omega dt+\int_{T_i}^{T_f}\int_{\Omega}\chi(\phi)\boldsymbol{u}\cdot\boldsymbol{v}\ d\Omega dt+\int_{\Omega}(\boldsymbol{u}\cdot\boldsymbol{v})|_{t=T_i}\ d\Omega \\
& +\int_{T_i}^{T}\int_{\Gamma_{\text{in}}\cup\Gamma_{\text{wall}}}\boldsymbol{u}\cdot\boldsymbol{v}\ d\Gamma dt+\int_{T_i}^{T_f}\int_{\Gamma_{\text{out}}}(-p\boldsymbol{I}+\mu\nabla\boldsymbol{u})\boldsymbol{n}\cdot\boldsymbol{v}\ d\Gamma dt \\
= & 0. \qquad \text{(A.1)}
\end{aligned}
$$

According to the Lagrangian multiplier method [63], the Lagrangian $J(\boldsymbol{u},p;\phi)$ for the optimization problem in Equation (8) can be expressed as follows:

$$
J(\boldsymbol{u},p;\phi)=F(\boldsymbol{u};\phi)+e(\boldsymbol{u},p;\phi)-\lambda G+\frac{\Lambda}{2}G^2 \qquad \text{(A.2)}
$$

By setting $A = \frac{\mu}{2}\left[\nabla \boldsymbol{u} + (\nabla \boldsymbol{u})^T\right] : \left[\nabla \boldsymbol{u} + (\nabla \boldsymbol{u})^T\right]$ for Eq.(36), one can obtain the variational of J to $\boldsymbol{u}$:

$$\begin{aligned}\frac{\partial J}{\partial \boldsymbol{u}} \cdot \delta \boldsymbol{u} = &\int_{T_i}^{T_f} \int_{\Omega} \frac{\partial A}{\partial \boldsymbol{u}} \cdot \delta \boldsymbol{u} \; d\Omega dt + \int_{T_i}^{T_f} \int_{\Gamma_{\text{out}}} \frac{\partial A}{\partial \nabla \boldsymbol{u}} \boldsymbol{n} \cdot \delta \boldsymbol{u} \; d\Gamma dt \\ &- \int_{T_i}^{T_f} \int_{\Omega} (\nabla \cdot \frac{\partial A}{\partial \nabla \boldsymbol{u}}) \cdot \delta \boldsymbol{u} \; d\Omega dt \end{aligned} \tag{A.3}$$

and the variational of J to p:

$$\frac{\partial J}{\partial p} \delta p = \int_{T_i}^{T_f} \int_{\Omega} \frac{\partial A}{\partial p} \delta p \; d\Omega dt \tag{A.4}$$

The Lebesgue measure of $[T_i, T_f] \times \Gamma$ in $D \times [T_i, T_f]$ is zero, then

$$\int_{T_i}^{T_f} \int_{\Omega} \chi(\phi) \delta \boldsymbol{u} \cdot \boldsymbol{v} \; d\Omega dt = 0 \tag{A.5}$$

Based on the partial integration approach, the Gauss theory and $\delta \boldsymbol{u} = \boldsymbol{0}$ on $\Gamma_{\text{in}} \cup \Gamma_{\text{wall}}$, the following transformations are obtained:

$$\begin{aligned}\int_{T_i}^{T_f} \int_{\Omega} \nabla \delta \boldsymbol{u} \colon \nabla \boldsymbol{v} \; d\Omega dt &= \int_{T_i}^{T_f} \int_{\Omega} \nabla \cdot (\nabla \boldsymbol{v} \cdot \delta \boldsymbol{u}) d\Omega dt - \int_{T_i}^{T_f} \int_{\Omega} \nabla \boldsymbol{v} \cdot \delta \boldsymbol{u} \; d\Omega dt \\ &= \int_{T_i}^{T_f} \int_{\Gamma_{\text{out}}} (\nabla \boldsymbol{v}) \boldsymbol{n} \cdot \delta \boldsymbol{u} d\Gamma dt - \int_{T_i}^{T_f} \int_{\Omega} \nabla \boldsymbol{v} \cdot \delta \boldsymbol{u} \; d\Omega dt \end{aligned} \tag{A.6}$$

$$\begin{aligned}-\int_{T_i}^{T_f} \int_{\Omega} q \nabla \cdot \delta \boldsymbol{u} \; d\Omega dt &= -\int_{T_i}^{T_f} \int_{\Omega} \nabla \cdot (q \delta \boldsymbol{u}) d\Omega dt + \int_{T_i}^{T_f} \int_{\Omega} \nabla q \cdot \delta \boldsymbol{u} \; d\Omega dt \\ &= -\int_{T_i}^{T_f} \int_{\Gamma_{\text{out}}} q \boldsymbol{n} \cdot \delta \boldsymbol{u} \; d\Gamma dt + \int_{T_i}^{T_f} \int_{\Omega} \nabla q \cdot \delta \boldsymbol{u} \; d\Omega dt \end{aligned} \tag{A.7}$$

$$\begin{aligned}\int_{T_i}^{T_f} \int_{\Omega} (\boldsymbol{u} \cdot \nabla) \, \delta \boldsymbol{u} \cdot \boldsymbol{v} \; d\Omega dt &= \int_{T_i}^{T_f} \int_{\Omega} \nabla \cdot [\boldsymbol{u} \cdot (\boldsymbol{v} \cdot \delta \boldsymbol{u})] \; d\Omega dt - \int_{T_i}^{T_f} \int_{\Omega} (\boldsymbol{u} \cdot \nabla) \, \boldsymbol{v} \cdot \delta \boldsymbol{u} d\Omega dt \\ &= \int_{T_i}^{T_f} \int_{\Gamma_{\text{out}}} (\boldsymbol{u} \cdot \boldsymbol{n}) \, \boldsymbol{v} \cdot \delta \boldsymbol{u} \; d\Gamma dt - \int_{T_i}^{T_f} \int_{\Omega} (\boldsymbol{u} \cdot \nabla) \, \boldsymbol{v} \cdot \delta \boldsymbol{u} \; d\Omega dt \end{aligned} \tag{A.8}$$

$$\int_{T_i}^{T_f} \int_{\Omega} (\delta \boldsymbol{u} \cdot \nabla) \, \boldsymbol{u} \cdot \boldsymbol{v} \; d\Omega dt = \int_{T_i}^{T_f} \int_{\Omega} (\nabla \boldsymbol{u}) \, \boldsymbol{v} \cdot \delta \boldsymbol{u} \; d\Omega dt \tag{A.9}$$

Therefore, the variational of J' to $\boldsymbol{u}$ is the following:

$$\begin{aligned}
\frac{\partial J}{\partial \boldsymbol{u}} \cdot \delta \boldsymbol{u} &= \frac{\partial F}{\partial \boldsymbol{u}} \cdot \delta \boldsymbol{u} + \frac{\partial e}{\partial \boldsymbol{u}} \cdot \delta \boldsymbol{u} \\
&= \int_{T_i}^{T_f} \int_{\Omega} \frac{\partial A}{\partial \boldsymbol{u}} \cdot \delta \boldsymbol{u} \; d\Omega dt + \int_{T_i}^{T_f} \int_{\Gamma_{\text{out}}} \frac{\partial A}{\partial \nabla \boldsymbol{u}} \boldsymbol{n} \cdot \delta \boldsymbol{u} \; d\Gamma dt \\
&\quad - \int_{T_i}^{T_f} \int_{\Omega} (\nabla \cdot \frac{\partial A}{\partial \nabla \boldsymbol{u}}) \cdot \delta \boldsymbol{u} \; d\Omega dt + \rho \int_{\Omega} [(\delta \boldsymbol{u} \cdot \boldsymbol{v})|_{t=T} - (\delta \boldsymbol{u} \cdot \boldsymbol{v})|_{t=T_i}] d\Omega \\
&\quad - \rho \int_{T_i}^{T_f} \int_{\Omega} \delta \boldsymbol{u} \cdot \frac{\partial \boldsymbol{v}}{\partial t} \; d\Omega dt + \rho \int_{T_i}^{T_f} \int_{\Gamma_{\text{out}}} (\boldsymbol{u} \cdot \boldsymbol{n}) \, \boldsymbol{v} \cdot \delta \boldsymbol{u} \; d\Gamma dt \\
&\quad - \rho \int_{T_i}^{T_f} \int_{\Omega} (\boldsymbol{u} \cdot \nabla) \, \boldsymbol{v} \cdot \delta \boldsymbol{u} \; d\Omega dt + \rho \int_{T_i}^{T_f} \int_{\Omega} (\nabla \boldsymbol{u}) \, \boldsymbol{v} \cdot \delta \boldsymbol{u} \; d\Omega dt \\
&\quad + \mu \int_{T_i}^{T_f} \int_{\Gamma_{\text{out}}} (\nabla \boldsymbol{v}) \boldsymbol{n} \cdot \delta \boldsymbol{u} \; d\Gamma dt - \mu \int_{T_i}^{T_f} \int_{\Omega} \nabla \boldsymbol{v} \cdot \delta \boldsymbol{u} \; d\Omega dt \\
&\quad - \int_{T_i}^{T_f} \int_{\Omega} \frac{\partial \boldsymbol{f}}{\partial \boldsymbol{u}} \cdot \delta \boldsymbol{u} \; d\Omega dt - \int_{T_i}^{T_f} \int_{\Gamma_{\text{out}}} q \boldsymbol{n} \cdot \delta \boldsymbol{u} \; d\Gamma dt + \int_{T_i}^{T_f} \int_{\Omega} \nabla q \cdot \delta \boldsymbol{u} \; d\Omega dt \\
&= \int_{T_i}^{T_f} \int_{\Omega} [-\rho \frac{\partial \boldsymbol{v}}{\partial t} - \rho \, (\boldsymbol{u} \cdot \nabla) \, \boldsymbol{v} + \rho \, (\nabla \boldsymbol{u}) \cdot \boldsymbol{v} - \mu \nabla^2 \boldsymbol{v} + \nabla q + \left(\frac{\partial A}{\partial \boldsymbol{u}} - \nabla \cdot \frac{\partial A}{\partial \nabla \boldsymbol{u}} \right) - \frac{\partial \boldsymbol{f}}{\partial \boldsymbol{u}}] \cdot \delta \boldsymbol{u} \; d\Omega dt \\
&\quad + \int_{T_i}^{T_f} \int_{\Gamma_{\text{out}}} [(-q \boldsymbol{I} + \mu \nabla \boldsymbol{u}) \boldsymbol{n} + \rho \, (\boldsymbol{u} \cdot \boldsymbol{n}) \, \boldsymbol{v} + \frac{\partial A}{\partial \nabla \boldsymbol{u}} \boldsymbol{n}] \cdot \delta \boldsymbol{u} \; d\Gamma dt + \rho \int_{\Omega} \boldsymbol{v}(T_f) \cdot \delta \boldsymbol{u} \; d\Omega
\end{aligned} \tag{A.10}$$

and the variational of J' to p is the following:

$$\begin{aligned}
\frac{\partial J}{\partial p} \delta p &= \frac{\partial F}{\partial p} \delta p + \frac{\partial e}{\partial p} \delta p \\
&= \int_{T_i}^{T_f} \int_{\Omega} \frac{\partial A}{\partial p} \delta p \; d\Omega dt + \int_{T_i}^{T_f} \int_{\Omega} (-\nabla \cdot \boldsymbol{v}) \delta p \; d\Omega dt \\
&\quad - \int_{T_i}^{T_f} \int_{\Omega} \frac{\partial \boldsymbol{f}}{\partial p} \cdot \boldsymbol{v} \delta p \; d\Omega dt + \int_{T_i}^{T_f} \int_{\Gamma_{\text{in}} \cup \Gamma_{\text{wall}}} \boldsymbol{v} \delta p \; d\Gamma dt \\
&= \int_{T_i}^{T_f} \int_{\Omega} (-\nabla \cdot \boldsymbol{v} + \frac{\partial A}{\partial p} p - \frac{\partial \boldsymbol{f}}{\partial p} \cdot \boldsymbol{v}) \delta p \; d\Omega dt + \int_{T_i}^{T_f} \int_{\Gamma_{\text{in}} \cup \Gamma_{\text{wall}}} \boldsymbol{v} \delta p \; d\Gamma dt
\end{aligned} \tag{A.11}$$

According to Karush-Kuhn-Tucker conditions [61], the variational of J' to $\boldsymbol{u}$ and the variational of J' to p should be zero corresponding to the optimal distribution of the level set function. Considering the arbitrariness of $\delta \boldsymbol{u}$ and δp, the adjoint equations of the Navier-Stokes equations for the optimization

problem can be obtained as in Eq.s(31)∼(35). In addition, considering the condition that the variational of J' to $\boldsymbol{u}$ is zero, one can obtain the sensitivity as in Eq. (40).

References

[1] M. P. Bendsøe, N. Kikuchi, Generating optimal topologies in structural design using a homogenization method, Computer Methods in Applied Mechanics and Engineering 71 (2) (1988) 197–224.

[2] M. P. Bendsøe, Topology optimization, in: Encyclopedia of Optimization, Springer, 2001, pp. 2636–2638.

[3] A. Cherkaev, Variational methods for structural optimization, Vol. 140, Springer Science & Business Media, 2012.

[4] F. Murat, Optimality conditions and homogenization, Nonlinear Variational Problems Pitman Publishing Program (1985) 1–8.

[5] M. P. Bendsøe, O. Sigmund, Material interpolation schemes in topology optimization, Archive of Applied Mechanics 69 (9-10) (1999) 635–654.

[6] G. Allaire, F. Jouve, A.-M. Toader, A level-set method for shape optimization, Comptes Rendus Mathematique 334 (12) (2002) 1125–1130.

[7] M. Y. Wang, X. Wang, D. Guo, A level set method for structural topology optimization, Computer Methods in Applied Mechanics and Engineering 192 (1-2) (2003) 227–246.

[8] G. Allaire, F. Jouve, A.-M. Toader, Structural optimization using sensitivity analysis and a level-set method, Journal of Computational Physics 194 (1) (2004) 363–393.

[9] H.-K. Zhao, T. Chan, B. Merriman, S. Osher, A variational level set approach to multiphase motion, Journal of Computational Physics 127 (1) (1996) 179–195.

[10] T. Borrvall, J. Petersson, Topology optimization of fluids in Stokes flow, International Journal for Numerical Methods in Fluids 41 (1) (2003) 77–107.

[11] N. Aage, T. H. Poulsen, A. Gersborg-Hansen, O. Sigmund, Topology optimization of large scale Stokes flow problems, Structural and Multidisciplinary Optimization 35 (2) (2008) 175–180.

[12] L. H. Olesen, F. Okkels, H. Bruus, A high-level programming-language implementation of topology optimization applied to steady-state Navier–Stokes flow, International Journal for Numerical Methods in Engineering 65 (7) (2006) 975–1001.

[13] Y. Deng, Z. Liu, P. Zhang, Y. Liu, Y. Wu, Topology optimization of unsteady incompressible Navier–Stokes flows, Journal of Computational Physics 230 (17) (2011) 6688–6708.

[14] S. Kreissl, K. Maute, Levelset based fluid topology optimization using the extended finite element method, Structural and Multidisciplinary Optimization 46 (3) (2012) 311–326.

[15] C. B. Dilgen, S. B. Dilgen, D. R. Fuhrman, O. Sigmund, B. S. Lazarov, Topology optimization of turbulent flows, Computer Methods in Applied Mechanics and Engineering 331 (2018) 363–393.

[16] S. B. Dilgen, C. B. Dilgen, D. R. Fuhrman, O. Sigmund, B. S. Lazarov, Density based topology optimization of turbulent flow heat transfer systems, Structural and Multidisciplinary Optimization 57 (5) (2018) 1905–1918.

[17] K. Yaji, T. Yamada, M. Yoshino, T. Matsumoto, K. Izui, S. Nishiwaki, Topology optimization using the lattice Boltzmann method incorporating level set boundary expressions, Journal of Computational Physics 274 (2014) 158–181.

[18] F. Dugas, Y. Favennec, C. Josset, Y. Fan, L. Luo, Topology optimization of thermal fluid flows with an adjoint Lattice Boltzmann Method, Journal of Computational Physics 365 (2018) 376–404.

[19] S. Nørgaard, O. Sigmund, B. Lazarov, Topology optimization of unsteady flow problems using the lattice boltzmann method, Journal of Computational Physics 307 (2016) 291–307.

[20] J. A. Sethian, A. Wiegmann, Structural boundary design via level set and immersed interface methods, Journal of Computational Physics 163 (2) (2000) 489–528.

[21] S. Osher, F. Santosa, Level set methods for optimization problems involving geometry and constraints: I. frequencies of a two-density inhomogeneous drum, Journal of Computational Physics 171 (1) (2001) 272–288.

[22] A. Leitão, O. Scherzer, On the relation between constraint regularization, level sets, and shape optimization, Inverse Problems 19 (1) (2003) L1.

[23] S. Amstutz, H. Andrä, A new algorithm for topology optimization using a level-set method, Journal of Computational Physics 216 (2) (2006) 573–588.

[24] S. Osher, J. Sethian, Fronts propagating with curvature-dependent speed: algorithms based on hamilton-jacobi formulations, Journal of Computational Physics 79 (1) (1988) 12–49.

[25] V. J. Challis, J. K. Guest, Level set topology optimization of fluids in Stokes flow, International Journal for Numerical Methods in Engineering 79 (10) (2009) 1284–1308.

[26] X. Duan, Y. Ma, R. Zhang, Optimal shape control of fluid flow using variational level set method, Physics Letters A 372 (9) (2008) 1374–1379.

[27] S. Zhou, Q. Li, A variational level set method for the topology optimization of steady-state Navier–Stokes flow, Journal of Computational Physics 227 (24) (2008) 10178–10195.

[28] X.-B. Duan, Y.-C. Ma, R. Zhang, Shape-topology optimization for Navier–Stokes problem using variational level set method, Journal of Computational and Applied Mathematics 222 (2) (2008) 487–499.

[29] Y. Deng, P. Zhang, Y. Liu, Y. Wu, Z. Liu, Optimization of unsteady incompressible Navier–Stokes flows using variational level set method, International Journal for Numerical Methods in Fluids 71 (12) (2013) 1475–1493.

[30] T. Yamada, K. Izui, S. Nishiwaki, A. Takezawa, A topology optimization method based on the level set method incorporating a fictitious interface energy, Computer Methods in Applied Mechanics and Engineering 199 (45-48) (2010) 2876–2891.

[31] K. Yaji, T. Yamada, K. Izui, S. Nishiwaki, Topology Optimization Method Using Level Set Boundary Expressions in Navier Stokes Flow, in: 12th AIAA Aviation Technology, Integration, and Operations (ATIO) Conference and 14th AIAA/ISSMO Multidisciplinary Analysis and Optimization Conference, 2012, p. 5526.

[32] K. Yaji, T. Yamada, M. Yoshino, T. Matsumoto, K. Izui, S. Nishiwaki, Topology optimization in thermal-fluid flow using the lattice Boltzmann method, Journal of Computational Physics 307 (2016) 355–377.

[33] C. Othmer, A continuous adjoint formulation for the computation of topological and surface sensitivities of ducted flows, International Journal for Numerical Methods in Fluids 58 (8) (2008) 861–877.

[34] S. Koshizuka, Y. Oka, Moving-particle semi-implicit method for fragmentation of incompressible fluid, Nuclear Science and Engineering 123 (3) (1996) 421–434.

[35] N. Mitsume, S. Yoshimura, K. Murotani, T. Yamada, Mps–fem partitioned coupling approach for fluid–structure interaction with free surface flow, International Journal of Computational Methods 11 (04) (2014) 1350101.

[36] K. Liao, C. Hu, A coupled fdm–fem method for free surface flow interaction with thin elastic plate, Journal of Marine Science and Technology 18 (1) (2013) 1–11.

[37] C. Körner, M. Thies, T. Hofmann, N. Thürey, U. Rüde, Lattice boltzmann model for free surface flow for modeling foaming, Journal of Statistical Physics 121 (1-2) (2005) 179–196.

[38] L. B. Lucy, A numerical approach to the testing of the fission hypothesis, The Astronomical Journal 82 (1977) 1013–1024.

[39] J. J. Monaghan, Smoothed particle hydrodynamics, Annual Review of Astronomy and Astrophysics 30 (1) (1992) 543–574.

[40] S. Koshizuka, H. Ikeda, Y. Oka, Numerical analysis of fragmentation mechanisms in vapor explosions, Nuclear Engineering and Design 189 (1-3) (1999) 423–433.

[41] S. Koshizuka, Application of moving particle semi-implicit method to nuclear reactor safety, Comput. Fluid Dynamics J. 9 (2001) 366–375.

[42] H. Xie, S. Koshizuka, Y. Oka, Simulation of drop deposition process in annular mist flow using three-dimensional particle method, Nuclear Engineering and Design 235 (16) (2005) 1687–1697.

[43] W. Tian, Y. Ishiwatari, S. Ikejiri, M. Yamakawa, Y. Oka, Numerical computation of thermally controlled steam bubble condensation using moving particle semi-implicit (mps) method, Annals of Nuclear Energy 37 (1) (2010) 5–15.

[44] H. Gotoh, T. Sakai, Lagrangian simulation of breaking waves using particle method, Coastal Engineering Journal 41 (3-4) (1999) 303–326.

[45] H. Gotoh, H. Ikari, T. Memita, T. Sakai, Lagrangian particle method for simulation of wave overtopping on a vertical seawall, Coastal Engineering Journal 47 (2-3) (2005) 157–181.

[46] H. Gotoh, T. Sakai, Key issues in the particle method for computation of wave breaking, Coastal Engineering 53 (2-3) (2006) 171–179.

[47] K. Shibata, S. Koshizuka, Numerical analysis of shipping water impact on a deck using a particle method, Ocean Engineering 34 (3-4) (2007) 585–593.

[48] M. Sueyoshi, M. Kashiwagi, S. Naito, Numerical simulation of wave-induced nonlinear motions of a two-dimensional floating body by the moving particle semi-implicit method, Journal of Marine Science and Technology 13 (2) (2008) 85–94.

[49] K. Shibata, S. Koshizuka, K. Tanizawa, Three-dimensional numerical analysis of shipping water onto a moving ship using a particle method, Journal of Marine Science and Technology 14 (2) (2009) 214–227.

[50] S. Shao, H. Gotoh, Turbulence particle models for tracking free surfaces, Journal of Hydraulic Research 43 (3) (2005) 276–289.

[51] A. Khayyer, H. Gotoh, On particle-based simulation of a dam break over a wet bed, Journal of Hydraulic Research 48 (2) (2010) 238–249.

[52] Y. Chikazawa, S. Koshizuka, Y. Oka, A particle method for elastic and visco-plastic structures and fluid-structure interactions, Computational Mechanics 27 (2) (2001) 97–106.

[53] S. Heo, S. Koshizuka, Y. Oka, Numerical analysis of boiling on high heat-flux and high subcooling condition using mps-mafl, International Journal of Heat and Mass Transfer 45 (13) (2002) 2633–2642.

[54] Z. Sun, G. Xi, X. Chen, Mechanism study of deformation and mass transfer for binary droplet collisions with particle method, Physics of Fluids 21 (3) (2009) 032106.

[55] K. Tsubota, S. Wada, H. Kamada, Y. Kitagawa, R. Lima, T. Yamaguchi, A particle method for blood flow simulation: application to flowing red blood cells and platelets, Journal of the Earth Simulator (2006) 2–7.

[56] K. Tsubota, S. Wada, Effect of the natural state of an elastic cellular membrane on tank-treading and tumbling motions of a single red blood cell, Physical Review E 81 (1) (2010) 011910.

[57] Z. Sun, G. Xi, X. Chen, A numerical study of stir mixing of liquids with particle method, Chemical Engineering Science 64 (2) (2009) 341–350.

[58] S. Koshizuka, A. Nobe, Y. Oka, Numerical analysis of breaking waves using the moving particle semi-implicit method, International Journal for Numerical Methods in Fluids 26 (7) (1998) 751–769.

[59] R. M. Errico, What is an adjoint model?, Bulletin of the American Meteorological Society 78 (11) (1997) 2577–2592.

[60] E. Sánchez-Palencia, Non-homogeneous media and vibration theory, Lecture Notes in Physics 127.

[61] M. Hinze, R. Pinnau, M. Ulbrich, S. Ulbrich, Optimization with PDE constraints, Vol. 23, Springer Science & Business Media, 2008.

[62] M. B. Giles, N. A. Pierce, An introduction to the adjoint approach to design, Flow, turbulence and combustion 65 (3-4) (2000) 393–415.

[63] S. Wright, J. Nocedal, Numerical optimization, Springer Science 35 (67-68) (1999) 7.

[64] J. K. Guest, J. H. Prévost, Topology optimization of creeping fluid flows using a Darcy–Stokes finite element, International Journal for Numerical Methods in Engineering 66 (3) (2006) 461–484.

[65] K. Ito, K. Kunisch, Lagrange multiplier approach to variational problems and applications, Vol. 15, Siam, Philadelphia, 2008.

[66] N. K. Yamaleev, B. Diskin, E. J. Nielsen, Local-in-time adjoint-based method for design optimization of unsteady flows, Journal of Computational Physics 229 (14) (2010) 5394–5407.

[67] Y. Yamada, M. Sakai, S. Mizutani, S. Koshizuka, M. Oochi, K. Murozono, Numerical simulation of three-dimensional free-surface flows with explicit moving particle simulation method, Transactions of the atomic energy society of Japan 10 (3) (2011) 185–193.